RESEARCH PAPER

Large-scale synthesis of 3D ordered microporous carbon at low temperature using cobalt ions exchanged zeolite Y as a template

Hong-Wei Zhao[1], Li-Xiang Li[1,2,*], Huai-Yang Zuo[1], Di Qu[1], Han Zhang[1], Lin Tao[1], Cheng-Guo Sun[1,3], Dong-Ying Ju[2], Bai-Gang An[1,2,*]

[1]Key Laboratory of Energy Materials and Electrochemistry Research Liaoning Province, School of Chemical Engineering, University of Science and Technology Liaoning, Anshan 114051, China;
[2]Hainan Provincial Key Lab of Fine Chemistry, School of Chemical Engineering and Technology, Hainan University, Haikou 570228, China;
[3]School of Chemical Engineering, Nanjing University of Science and Technology, Nanjing 210094, China

Abstract: Zeolite-templated carbons (ZTCs) have a unique three-dimensional (3D) ordered microporous structure and an extra-large surface area, and have excellent properties in adsorption and energy storage. Unfortunately, the lack of efficient synthesis strategies and the difficulty of doing this on a large-scale have seriously limited their development. We have developed a large-scale simple production route using a relatively low synthesis temperature and direct acetylene chemical vapor deposition (CVD) using Co ion-exchanged zeolite Y (CoY) as the template. The Co^{2+} confined in the zeolite acts as Lewis acid sites to catalyze the pyrolysis of acetylene through the d-π coordination effect, making carbon deposition occur selectively inside the zeolite at 400 °C rather than on the external surface. By systematically investigating the CVD temperature and time, the optimum conditions of 8 h deposition at 400 °C produces an excellent 3D ordered-microporous structure and outstanding structure parameters (3 000 $m^2\ g^{-1}$, 1.33 $cm^3\ g^{-1}$). Its CO_2 adsorption capacity and selectivity are 2.78 mmol g^{-1} (25 °C, 100 kPa) and 98, respectively. This simple CVD process allows the synthesis of high-quality ZTCs on a large scale at a low cost.
Key Words: Zeolite-templated carbon; Cobalt ion-exchanged; Low temperature chemical vapor deposition; Ordered microporous; CO_2 adsorbent

1 Introduction

Nanoporous carbons are one of the hottest topics in physics, chemistry, and materials science. In the past 30 years, many novel carbon nanomaterials with unique structures and properties have emerged, including CNTs, graphene, graphdiyne, graphite-like porous carbon, and carbon nanocages[1-5]. The practical and potential applications of nanoporous carbons in adsorption, catalysis, energy, environment, sensors, and optoelectronic devices aroused great interest in academia and industry[5-10]. Various properties of porous carbon materials are highly related to their nanostructure[11-13]. Much effort has been made to design and tune the nanostructure, especially the pore structure of carbon materials[14-16]. However, it remains a significant challenge to accurately construct the pores that are ordered distribution in three dimensions (3D) and with a pore size of about 1.0 nm in carbon materials. Zeolite, as a crystalline porous material with a well-defined molecular level, has been attracting much attention owing to its micropore size and ordered distribution in 3D[17]. It would be fascinating if such an ordered microporous structure of zeolite could combine with the advantages of carbon materials, such as good conductivity, mechanical flexibility, and facile chemical modification[18-25]. Duplicating zeolite by using itself as a template is an ideal route to get the carbon material with an ordered nanostructure. The bottlenecks are making carbon precursors filling into the zeolite pores with tiny sizes and obtaining a stable and ordered pore structure constructed by carbons after template removal. The first successful attempt to synthesize zeolite-templated carbons (ZTCs) was made by Kyotani's group in 1997[26]. They first used the impregnation of zeolite with furfuryl alcohol (FA) or propylene CVD method to prepare ZTCs, but the quality was poor[26]. Subsequently, they further optimized the preparation conditions and successfully obtained high specific surface areas (SSA) of 3000-4000 $m^2\ g^{-1}$ by a two-step method (FA impregnation followed by CVD)[27-29]. However, almost 5 days for molecular filling and polymerization causes a long time to consume, making the commercial application of ZTCs impossible from the view of technology, yield and cost.
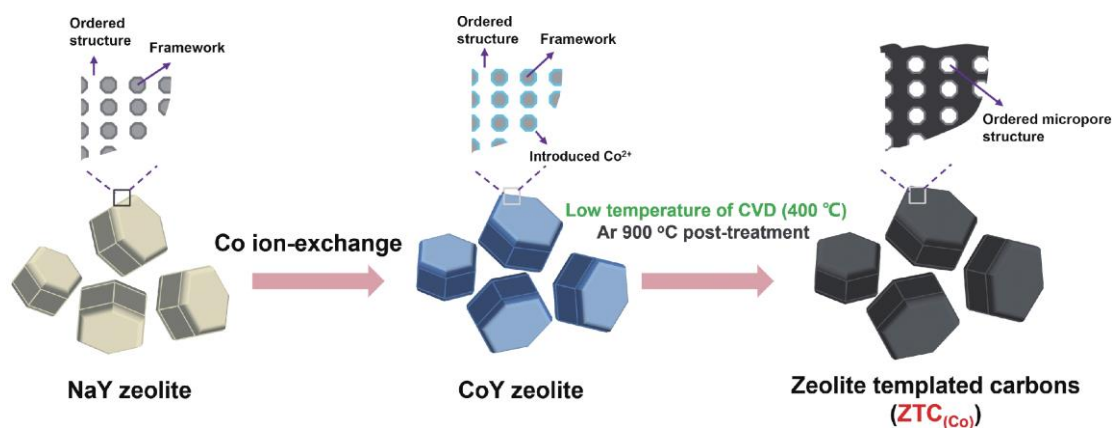
Scheme 1   Schematic diagram for the synthesis of ZTC(Co) and in-situ CNTs/ ZTC(Co) by using CoY zeolite as a template and acetylene as a carbon source

Compared with the strict and time-consuming process of filling and polymerizing small organic molecules to prepare ZTCs, direct CVD technology is easy to control and can continuously produce carbon materials and thus attempt to prepare ZTCs. The technique of direct CVD to synthesize ZTCs was first reported by Kyotani's group, the SSA of ZTCs is 2760 $m^2 g^{-1}$ by acetylene CVD at 600 °C[30]. Nonetheless, direct CVD technology still faces poor structural integrity, the high cost caused by high temperatures, and the inability to prepare high-quality ZTCs on a large scale, thus limiting its practical application. Therefore, if the carbon precursor could be selectively deposited into the zeolite pores at a temperature lower than its pyrolysis temperature in the CVD process, it is beneficial for the large-scale preparation of high-quality ZTCs. In our previous works, the silanization method enhanced the activity of carbon deposition onto the wall of pores of the zeolite Y template. Direct CVD of acetonitrile vapor successfully synthesized N-doped ZTCs with ordered microporous structures[31]. Although this method failed to resolve the problem of high-temperature CVD, it suggests that modifying the zeolite template could be a valid route to improve the nanostructure of ZTCs as prepared by a direct CVD.

Among the works using template modification to improve the nanostructure of carbon materials, Ryoo's group contributed a pioneering study[32-33]. They made La^{3+} cations embedded in zeolite pores by the ion exchange method. The embedded La^{3+} as catalytic sites make carbon-containing precursors pyrolyzed selectively inside the pores without the coke on the external surface of zeolite at a temperature as low as 600 °C. As a suitable Lewis acid catalyst, the transition metal cation would bond with hydrocarbon molecules through d-π coordination. Using the transition metal ions (Co^{2+}, Mn^{2+}, Cu^{2+} and Ni^{2+}) exchanged zeolite as a template, microporous carbon with well ordered-structure in 3D can be produced by the direct CVD of ethylene or acetylene accompanied with water vapor[34]. Cobalt and its compounds are the most commonly used catalysts for synthesizing carbon materials. In principle, Co ions have vacant d orbitals in the electron shell structures. The d-π interactions directly stabilize hydrocarbons and catalyze the formation of

carbon frameworks during pyrocondensation without other additional conditions. Using Co^{2+} ion-exchanged zeolite as a template, ZTCs with ordered nanostructure were synthesized by CVD of ethylene, adding water vapor at 600 °C[34]. However, introducing water vapor in the CVD process caused the oxidation of carbon to produce the oxygen-containing groups around the porous carbons. Consequently, it induces the decreases in pore orderliness and SSA.

Herein, the ZTCs with good nanostructure prepared using Co^{2+} ion-exchanged zeolite as a template by the direct acetylene CVD as shown in Scheme 1. The pyrolysis of acetylene and carbon deposition into micropores of CoY zeolite efficiently operated at a temperature as low as 400 °C, which is a lower temperature for synthesizing ZTCs than the traditional CVD methods. By optimizing the preparation parameters, the optimal $ZTC_{(Co)}$-400-8h (Co^{2+} ion-exchanged zeolite as template and acetylene 8 h CVD at 400 °C) owns an excellent 3D ordered-microporous structure and significant SSA (3 000 $m^2 g^{-1}$), the improvement of structural integrity is beneficial to improve the CO_2 adsorption capacity and selectivity. The simple CVD technology also allows a large-scale synthesis of high-quality ZTCs, up to 10.0 g CoY zeolite could be replicated into high-quality ZTCs.

2   Experimental

2.1   Chemicals and reagents

The NaY zeolite ($SiO_2/Al_2O_3 \geq 5.3$, $Na_2O \leq 12.5\%$) was obtained from Nanjing XFNANO Materials Tech Co., Ltd. Cobalt sulfate heptahydrate ($CoSO_4 \cdot 7H_2O$, $\geq 99.5\%$), hydrochloric acid (HCl, 5.0 mol L^{-1}), hydrofluoric acid (HF, $\geq 40\%$) were purchased from Sinopharm Chemical Reagent Co., Ltd. Ultrapure acetylene (C_2H_2, $\geq 99.999\%$), nitrogen (N_2, $\geq 99.999\%$), argon (Ar, $\geq 99.999\%$) and carbon dioxide (CO_2, $\geq 99.999\%$) were supplied by the Anshan Angang gas Limited Liability Company.

2.2   Synthesis of Co ions-exchanged zeolite

Co^{2+} exchange was performed using 3.0 g Y zeolite in 0.1 mol L^{-1} 180 mL aqueous solution of $CoSO_4$. The mixed solution was kept at 60 °C for 3 h under reduced pressure, and

the treatment process of ion exchange was repeated twice. The resulting slurry was filtered and thoroughly washed with distilled water and then dried for 12 h in a vacuum oven at 80 °C. The name of the sample is CoY zeolite (before calcination). Then, CoY zeolite was calcined at 550 °C for 4 h in the air again.

2.3 Preparation of ZTCs by NaY and CoY zeolite

The ZTCs were synthesized using acetylene as a carbon source and NaY and CoY zeolite as a template, respectively. In a typical carbon synthesis process by chemical vapor deposition (CVD), 0.4 g of CoY (or NaY) zeolite was placed in a horizontal quartz reactor (50 mm inner diameter), and the air purged by pure Ar gas flow at room temperature with 1 h in the reactor. The CVD temperature of the synthesis device was heated up to 700 °C (CoY zeolite from 700 to 200 °C, and NaY zeolite from 700 to 500 °C, respectively, samples were collected every 100 °C) under pure Ar gas flow with a heating rate of 5 °C min^{-1}. Then acetylene gas (10% in Ar, acetylene: 5 mL min^{-1}; Ar: 45 mL min^{-1}) was passed through the reactor for 1 h. After the carbonaceous deposition, the graphitization temperature was increased to 900 °C and was maintained for 1 h under pure Ar gas again. After cooling to room temperature, the carbon compounds indicated as C/NaY-A-1h and C/CoY-A-1h, where the A denoted the CVD temperature (°C). Finally, the carbon composite of C/CoY-A-1h was treated with HF/HCl mixture solution to liberate the carbon product from the zeolite template. The final product was obtained by purifying with deionized water and drying in a 80 °C vacuum oven for one night. Finally, carbon samples were named ZTC$_{(Co)}$-A-1h. In addition, another set of carbon samples was synthesized by CoY zeolite through CVD at 400 °C with different CVD times (2, 4 and 8 h) of carbon deposition in the same synthesis device. Before and after HF/HCl mixture solution treatment, the samples were C/CoY-400-B and ZTC$_{(Co)}$-400-B, respectively, where the B denoted CVD time (h). For the large-scale synthesis of ZTC(Co), only the mass of CoY zeolite and CVD conditions were changed: the 10.0 g of CoY zeolite placed in a horizontal quartz reactor, and length, width, and height were 100, 17.5, 17.5 mm, respectively; 8 h at 400 °C CVD temperature (acetylene gas: 30 mL min^{-1}, Ar gas: 30 mL min^{-1}); 1 h at 900 °C graphitization temperature under pure Ar gas (100 mL min^{-1}). The final large-scale synthesized carbon sample was named ZTC$_{(Co)}$-400-8h(L).

2.4 Characterization

Thermogravimetric analysis (TGA, TA SDT-Q600, the ceramic crucible, heat rate of 10 °C min^{-1} in the air) was conducted due to the different water absorption capacity of the samples. The weight loss (%) of the samples is different at room temperature to 300 °C, so the TG curves of carbon contents were collected in the range of 300 to 900 °C. The morphology and structure of the catalysts were characterized using scanning electron microscopy (SEM, FEI Apreo, operated at 1 kV) and transmission electron microscopy (TEM, FEI Talos F200X, operated at 200 kV). The powder X-ray diffraction device (XRD, X'pret Powder, Rigaku D/MAX-2500X, Cu $K\alpha$) and

Raman spectrometer (HORIBA Xplora Plus, excited by 532 nm laser) were used to characterize the ordered structure and graphitization degree of samples. X-ray photoelectron spectroscopy (XPS, SHIMADZU, AXIS SUPRA, Al $K\alpha$) was used to analyze the chemical states of samples. N$_2$ adsorption measurements were measured at liquid nitrogen temperature (−196 °C) using a volumetric sorption analyzer (Micromeritics, ASAP 2020). Before the N$_2$ adsorption measurements, all samples were outgassed for 6 h at 300 °C in a vacuum. The specific surface area (SSA) was determined according to the Brunauer-Emmett-Teller (BET) method using adsorption data points in the pressure range of 0.01-0.05. Pore size distributions (PSDs) and pore volume were determined using non-local density functional theory (NLDFT), assuming the slit-shaped pore geometry. The micropore (Vmicro) volume was determined from the NLDFT cumulative volumes in the pore diameter range of $d \leq 2$ nm. The volume of the total pore (Vtotal) was determined at $p/p_0 = 0.96$.

2.5 Adsorption experiments

Static CO$_2$ and N$_2$ adsorption tests of samples were measured on a Micromeritics ASAP 2020 instrument under the pressure of 0-100 kPa at 0, 25 and 50 °C after samples that had been degassed at 120 °C for 12 h. The CO$_2$ adsorptions were measured on a range of temperatures (0, 25 and 50 °C) and pressures (0-100 kPa) with 20 mg samples. Meanwhile, the N$_2$ isotherms were measured at 25 °C and pressures (0-100 kPa) with 20 mg samples. The adsorbed quantities (mmol g^{-1}) were calculated from the measured pressures after equilibrium arrived. The isosteric heat of adsorption (Q_{st}) was from adsorption isotherms at 0, 25 and 50 °C, with the Clausius-Clapeyron equation[35]. The adsorption selectivity of CO$_2$/N$_2$ was obtained from CO$_2$ and N$_2$ isotherms at 298 K. The selectivity was calculated for CO^2/N^2=15/85 (up to 100 kPa) with ideal adsorbed solution theory (IAST) by using the free software[36]. The isotherms were fitted with the "Dual-site Langmuir-Freundlich Model" for selectivity calculations.

Dual-Site Langmuir-Freundlich (DSLF):

$$q = q_1 \frac{(k_1 P)^{n_1}}{1 + (k_1 P)^{n_1}} + q_2 \frac{(k_2 P)^{n_2}}{1 + (k_2 P)^{n_2}}$$

where q is the adsorbed amount per mass of adsorbent (mmol g^{-1}), P is the pressure of bulk gas pressure at equilibrium status (kPa), q_1 and q_2 are the saturation capacities (mmol g^{-1}), k_1 and k_2 are the affinity coefficients, n_1 and n_2 are the isotherm model parameter.

Assuming a binary gas mixture containing component 1 and component 2, the IAST selectivity (S) was defined as the following:

$$S = (\frac{q_1}{q_2})/(\frac{p_1}{p_2})$$

where q_1 (q_2) and p_1 (p_2) are the mole fractions of components 1 and 2 in the adsorbed and bulk phases.

3 Results and discussion

3.1 Preparation and structure of Co Ion-exchange template

As shown in Fig. S1a, the color changes of zeolite samples could be observed through the photographs. The color of NaY zeolite changes from white to pink after the process of Co^{2+} ion exchange and then turns to purple after 550 °C heat treatment. It indicates a successful ion exchange since the color of low concentrations of Co^{2+} is pink. After the heat treatment, the residual water in the zeolite template was evaporated completely, resulting in the increase of the concentration of Co^{2+}, and thus template turned purple. The X-ray photoelectron spectra (XPS) of the NaY and CoY zeolite are shown in Fig. 1a. In the CoY zeolite, Co 2p characteristic peak appears at 783.6 eV[37-38]. Accordingly, the peak intensity of Na 1s at 1 072.5 eV is weakened. It can be inferred that Co elements replace a part of Na elements in NaY zeolite after ion exchange, which proves that the Co element has been successfully exchanged into the zeolite. Small-angle XRD was used to investigate whether the process of preparing CoY zeolite would affect the original ordered pore structure of the zeolite. All zeolite samples contain (111) diffraction peaks around 2θ of 6°-7°, as shown in Fig. 1b, which proves that the intrinsically ordered nanostructure of zeolite was not destroyed by the modification processes[39-40]. After calcination, the more substantial peak of (111) zeolite indicates a higher structural order of CoY zeolite. The characteristic peaks of metallic Co were not observed in CoY zeolite (before calcination) and CoY zeolite (Fig. 1c), which indicates a stabilized Co^{2+} in the zeolite skeleton. All zeolite samples have similar morphology from the SEM observation (Fig. 1d-f), suggesting that the ion exchange process does not change the CoY zeolite inherited from the NaY zeolite template. In addition, there are no apparent metal clusters on the surface of CoY zeolite.

The N_2 adsorption isotherms of NaY and CoY zeolite are shown in Fig. S2a. Two samples have the type I isotherm characteristics representing the microporous materials[41-42]. The pore sizes of NaY and CoY zeolite concentrated at 0.7-1.0 nm, and the primary pore size of CoY zeolite is slightly smaller than NaY zeolite (Fig. S2b). The SSA and pore volume of CoY zeolite (572 m^2 g^{-1}, 0.28 cm^3 g^{-1}) are also slightly lower than that of NaY zeolite (649 m^2 g^{-1}, 0.33 cm^3 g^{-1}), as shown in Table S1. The main reason is that the heat treatment of 550 °C was used to stabilize the structure of CoY zeolite, it also resulted in the pore contraction of CoY zeolite.

3.2 The activity and efficiency of Co ion-exchange template for carbon deposition

The CVD temperature is crucial in ensuring pyrolysis and deposition of carbon precursors into CoY zeolite pores. Here, a direct CVD of acetylene using CoY and NaY zeolite as a template was carried out. The effects of CVD temperature (from 700 to 200 °C) on the pyrolysis of acetylene and carbon deposition were investigated. With the temperature decrease of acetylene CVD from 700 to 200 °C, the appearance color of C/CoY-A-1h ('A' means CVD temperature) samples were still black even at 300 °C (Fig. S1b). In contrast, the C/NaY-A-1h sample only turned brown at 500 °C (Fig. S1c), indicating that the CoY zeolite as a template has a higher carbon deposition activity than the NaY template. The effects of CVD temperature on carbon deposition into the zeolite template were further analyzed by TGA (Fig. 2a and S3). Using NaY zeolite, a valid carbon deposition only occurs at 600 °C, and carbon deposition is 10.3% (mass fraction) after 1 h. However, the deposition amount of carbon reaches 9.8% (mass fraction) even at 300 °C using CoY zeolite. Such a low temperature for carbon deposition is far lower than the temperature required by the conventional CVD method to synthesize carbon materials using acetylene precursors (ca. 600 °C) and propylene (ca. 700 °C)[30, 43-45]. In addition to a low temperature for the active
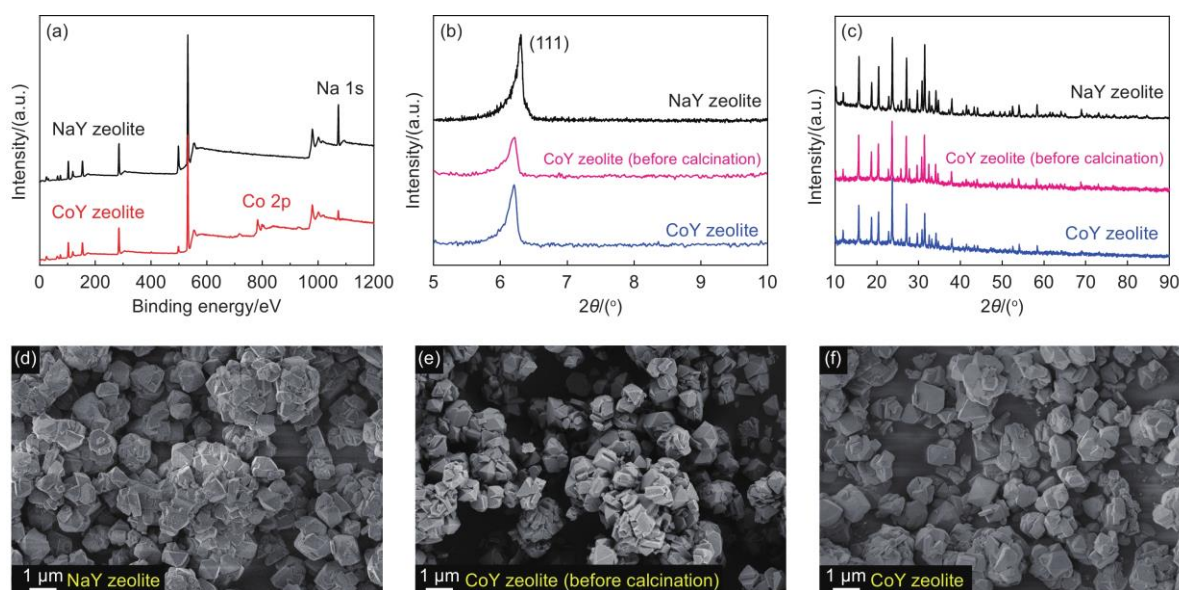

Fig. 1 (a) XPS survey spectra of the NaY and CoY zeolite. (b) Small-angle and (c) wide-angle XRD patterns of the NaY zeolite, CoY zeolite (before calcination) and CoY zeolite. (d-f) SEM images of NaY zeolite, CoY zeolite (before calcination) and CoY zeolite, respectively
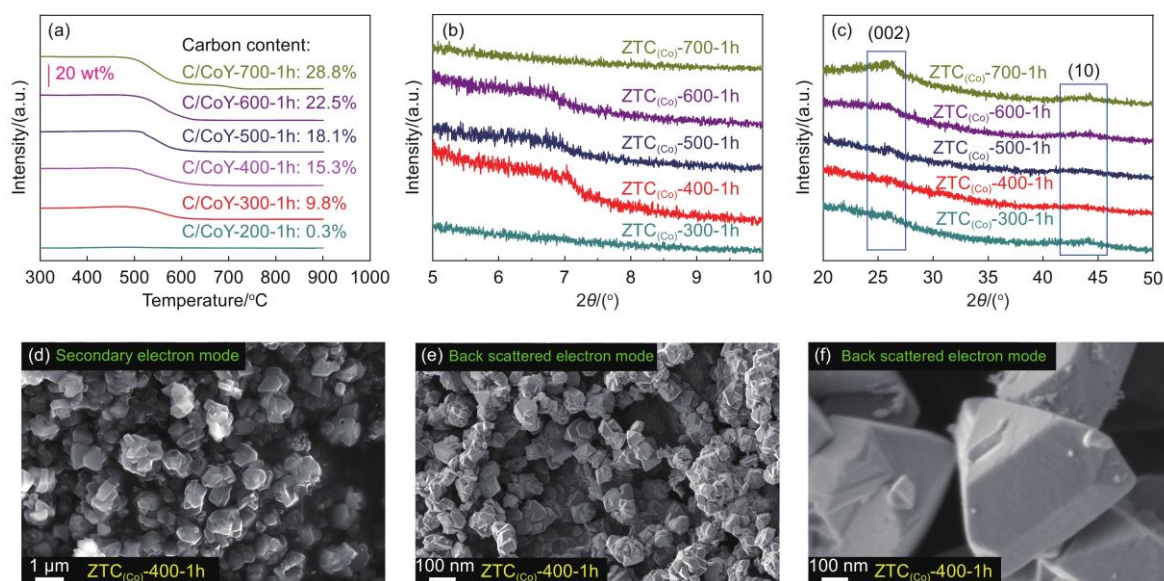
Fig. 2   (a) Amount of carbon deposition in the NaY and CoY zeolite plotted as a function of the different temperatures with using acetylene/Ar gas for 1 h. (b) Small-angle and (c) wide-angle XRD patterns of all $ZTC_{(Co)}$-A-1h samples. SEM images: (d) Secondary electron and (e, f) back scattered electron images of $ZTC_{(Co)}$-400-1h

deposition of carbon, using CoY zeolite as a template can also enhance the efficiency of carbon deposition. At the same CVD temperature, the deposition efficiency using CoY zeolite was significantly higher than NaY zeolite. As Moon et al. proposed in synthesizing 3D microporous carbon using Co ion-exchanged zeolite by CVD, Co^{2+} as the Lewis acid sites could form d-π coordination with acetylene[34]. Therefore, the CVD temperature for valid carbon deposition decreases, and the corresponding deposition efficiency increases. The Co^{2+} embedded in zeolite plays a critical catalytic site for acetylene pyrolysis and carbon deposition. The CVD temperature is also a key factor affecting the nanostructure of ZTCs.

After acid treatment, the XRD tests were used to analyze the structure of $ZTC_{(Co)}$-A-1h samples prepared at different temperatures. The weak characteristic peak at the low angle region around 2θ of 6°-7° is visible for all samples except $ZTC_{(Co)}$-700-1h and $ZTC_{(Co)}$-300-1h (Fig. 2b), which indicates the existence of a few completely ordered microporous structures. Furthermore, compared to the other samples, the 2 broad weak peaks representing carbon (002) and (10) around 26° and 44°, are hardly observed for $ZTC_{(Co)}$-400-1h[46, 47] (Fig. 2c). After acid treatment, the $ZTC_{(Co)}$-400-1h still showed a similarly particular morphology as the zeolite template (Fig. 2d-f).

3.3 Microstructure analysis of ZTCs

Raman spectra of all $ZTC_{(Co)}$-A-1h samples were deconvoluted into 4 components (Fig. S4). The corresponding curve-fitting results and the intensity ratio of the *D* and *G* bands (I_D/I_G) are shown in Fig. S5. Combined with TGA, XRD and SEM, the low I_D/I_G of ZTC-400-1h suggests that the $ZTC_{(Co)}$-400-1h has a good graphitization degree, which could be attributed to a large number of carbide-like compounds produced by the CVD process and growing along the active

nano-channels inside the zeolite template rather than the random growth of CNTs outside the zeolite at the higher CVD temperature. The TEM image (Fig. S6) shows the relatively well-ordered microporous structure of the $ZTC_{(Co)}$-400-1h. Notably, the ordered micropores are open, and carbon layers do not cover the outer surface. The acetylene was selectively deposited onto the active pore wall of CoY zeolite at a CVD temperature of 400 °C.

Pore structure and SSA of $ZTC_{(Co)}$-A-1h samples were examined by N_2 adsorption isotherms. All $ZTC_{(Co)}$-A-1h samples contain a high adsorption capacity at $p/p_0 \leq 0.1$, suggesting their characteristic of microporous structure (Fig. 3a). $ZTC_{(Co)}$-400-1h exhibited the highest adsorption capacity at $p/p_0 \leq 0.1$, demonstrating the highest microporous porosity, the most significant SSA of 2 200 m^2 g^{-1} and total pore volume of 1.00 cm^3 g^{-1} (Table S1). The PSD of Fig. 3b further illustrated the microporous feature of $ZTC_{(Co)}$-A-1h samples. Their pore size focuses on 1.2 nm, which results from the reverse replication of zeolite skeleton into carbon micropores. The pores distributed around 1.7-3.0 nm were ascribed to a part of zeolite pores that could finally interconnect after the acid treatment. Therefore, $ZTC_{(Co)}$-400-1h has an ordered pore structure. It could be extrapolated that the Co ions in CoY zeolite catalyze the acetylene conversed into the unstable carbide-like compounds at low temperature of 400 °C through d-π coordination and polymerization. After the heat treatment, the carbide-like compounds could be transformed into the stable solid carbon along the ordered microporous channels under the limitation of the template, thus forming a stable three-dimensional carbon structure. Although the SSA of $ZTC_{(Co)}$-400-1h has shown the orderliness of pore structure, the short CVD time of 1 h did not get the full carbon deposition into the pores of CoY zeolite. To obtain the highly ordered ZTCs with a large SSA, a reasonable amount of carbon deposition is a requisite
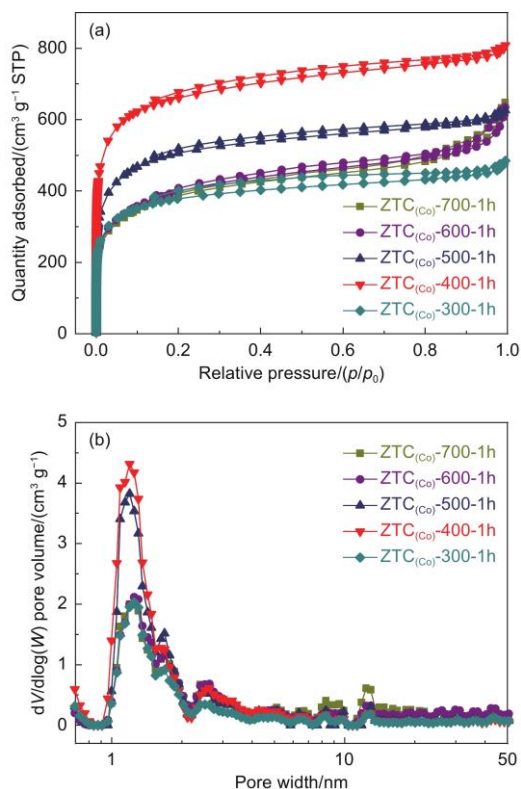
Fig. 3 (a) N₂ adsorption-desorption isotherms and (b) NLDFT pore size distribution of different ZTC(Co)-A-1h samples

by controlling the CVD time. The pore size around 1.7-3.0 nm are ascribed to a part of zeolite pores that could finally interconnect after the acid treatment. Therefore, ZTC(Co)-400-

1h has an ordered pore structure. It could be extrapolated that the Co ions in CoY zeolite catalyze the acetylene conversed into the unstable carbide-like compounds at low temperature of 400 °C through d-π coordination and polymerization. After the heat treatment, the carbide-like compounds could be transformed into the stable solid carbon along the ordered microporous channels under the limitation of the template, thus forming a stable three-dimensional carbon structure. Although the SSA of ZTC(Co)-400-1h has shown the orderliness of pore structure, the short CVD time of 1 h does not get the full carbon deposition into the pores of CoY zeolite. To obtain the highly ordered ZTCs with a large SSA, a reasonable amount of carbon deposition is a requisite by controlling the CVD time.

3.4 Optimization of the ordered structure of ZTCs

Carbon amount filling into the zeolite template is an essential factor in constructing a stable and ordered microstructure of high-quality ZTCs, which was feasible to prepare ZTCs by CVD at 400 °C. However, it needs further study on how CVD time influences the carbon deposition amount and the resulting microstructure of ZTCs. The time of CVD to prepare ZTCs was extended from 1.0 to 8.0 h, respectively. As shown by TGA curves in Fig. 4a, carbon content of the sample increases with CVD time. When CVD time was prolonged to 8.0 h, the carbon amount of C/CoY-400-8h could be up to 20.5% (mass fraction). The uniformly dispersed Co sites in the zeolite template could provide catalytic activity for the low-temperature acetylene carbonization, and the pore of template remains open for the
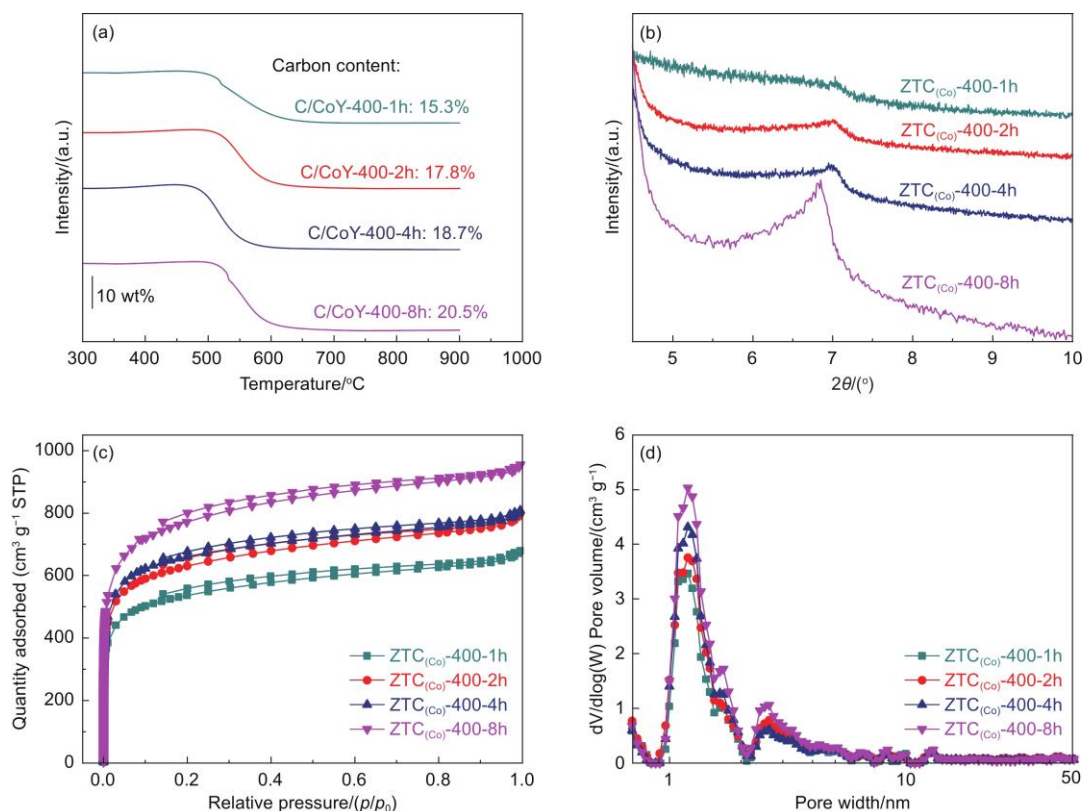

Fig. 4 (a) TGA curves of C/CoY-400-1h, C/CoY-400-2h, C/CoY-400-4h and C/CoY-400-8h. (b) Small-angle XRD patterns, (c) N₂ adsorption-desorption isotherms and (d) NLDFT pore size distribution of ZTC(Co)-400-1h, ZTC(Co)-400-2h, ZTC(Co)-400-4h and ZTC(Co)-400-8h

entrance of carbon precursor molecules. The carbon loading amount could achieve a high standard for building a robust and ordered microporous framework[25]. After the template removal, the small-angle and wide-angle XRD patterns of samples as shown in Fig. 4b and S7. The diffraction peak intensity of ZTC$_{(Co)}$-400-8h at 2θ of 6°-7° representing the ordered pore arrangement is significantly enhanced, suggesting that the increased carbon amount is mainly concentrated in the interior of the template to build the ordered and stable microporous structure. In the wide-angle XRD results (Fig. S7), the (002) peaks of the samples from ZTC$_{(Co)}$-400-1h to ZTC$_{(Co)}$-400-8h showed no changes significantly. It proves again that there is no deposition of dense carbon layers around the external surface of CoY zeolite. The N$_2$ adsorption isotherms and PSD curves (Fig. 4c-d) of samples demonstrate that ZTC$_{(Co)}$-400-8h has more micropores focused on 1.2 nm. As summarized in Table 1, the SSA and pore volume of ZTC$_{(Co)}$-400-8h could be up to 3 000 m^2 g^{-1} and 1.33 cm^3 g^{-1}, respectively. The high SSA and large pore volume are attributed to a more complete, internally ordered micropore structure.

As Raman spectroscopy shown in Fig. S8, the I_D/I_G value of ZTC$_{(Co)}$-400-8h (I_D/I_G =0.88) is slightly higher than the other samples. This abnormal phenomenon suggests an increase of defects and edge sites in the graphite structure of ZTCs. As a template, zeolite has a 3D interconnected pore with a pore size of less than 1.2 nm. It reversally duplicates that ZTCs with a

Table 1 The SSA and pore volume from the N$_2$ adsorption-desorption isotherms at -196 °C and synthesis condition for ZTC$_{(Co)}$-400-B

Samples	Time[a]	SSA[b]	V_1[c]	V_2[d]
ZTC$_{(Co)}$-400-1h	1	2200	1.00	0.80
ZTC$_{(Co)}$-400-2h	2	2390	1.05	0.82
ZTC$_{(Co)}$-400-4h	4	2520	1.11	0.87
ZTC$_{(Co)}$-400-8h	8	3000	1.33	1.03

well-ordered structure are constructed by the graphene layer with a large domain size deposited inside zeolite channels, which leads to many distortion sites at the pore junctions[48]. It is equivalent to a classical 2D sp^2 carbon network transformed into a 3D distortion network. The distortion locations are considered defects in graphite structure, which is why ZTC$_{(Co)}$-400-8h has the better-ordered structure but more "defects". Furthermore, the distortion locations could result in more edge sites that are easily bonded with O species. As shown by the XPS survey spectra of samples (Fig. S9), the prominent peaks of carbon (C 1s, 284.1 eV), oxygen (O 1s, 531.6 eV), and fluorine (F 1s, 688.8 eV) elements could be observed in all samples[34], the residual fluorine elements could be introduced by acid treatment. ZTC$_{(Co)}$-400-8h owns the highest oxygen content of 6.7 at% among the samples (Table S2).

The morphology and microstructure of ZTC$_{(Co)}$-400-8h are observed by SEM and TEM shown in Fig. 5. The extension
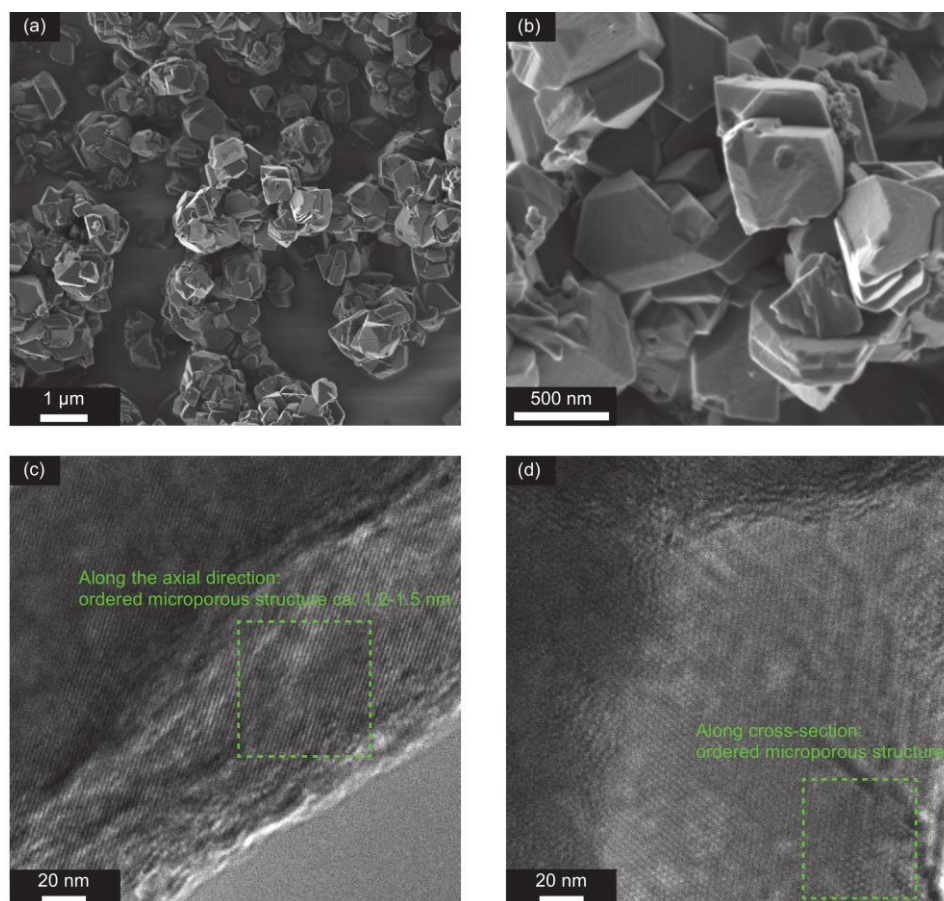

Fig. 5 (a, b) SEM images of ZTC$_{(Co)}$-400-8h, (c, d) TEM images of ZTC$_{(Co)}$-400-8h with different viewing directions

of the acetylene intake time to 8 h does not change the morphology of ZTCs inheriting from the CoY zeolite template. The sharp edges and corners of particles suggest less carbon deposition around the external surface of the template. As shown in TEM images, the higher carbon filling into the template improves the structural order degree of $ZTC_{(Co)}$-400-8h. The ordered distribution of micropores could be more clearly observed from the directions along and vertical the pore channels. The results further demonstrate that the ZTCs with highly ordered structures could be obtained by optimizing CVD time.

3.5 CO₂ adsorption property of ZTCs

Porous materials are widely used in the field of CO_2 storage and separation. Developing an application of ZTCs prepared by the CoY zeolite template, its CO_2 adsorption ability was investigated and evaluated by static CO_2 and N_2 adsorption tests. The adsorption isotherms of samples (Fig. 6a-d) show that the CO_2 adsorption capacity of all samples is much higher than their N_2 adsorption capacity, which is due to the higher quadrupole coupling and the faster gas diffusion rate of CO_2 than N_2 molecules, the CO_2 adsorbate could more effectively overcome diffusion obstacle and enter smaller pores under the

same adsorption condition[49-51]. In addition, CO_2 adsorption capacity decreases gradually with increasing temperature (0 to 50 °C), which could be attributed that the Langmuir parameter b decreases as temperature increases and the gas adsorption capacity also decreases according to the Langmuir adsorption model[52]. As shown by Fig. 6e, $ZTC_{(Co)}$-400-8h exhibits the highest CO_2 uptake (2.78 mmol g⁻¹), which should be attributed to the higher surface area (3 000 m² g⁻¹) and pore volume (1.33 cm³ g⁻¹) than other samples (Fig. 6f). Furthermore, the 3D ordered micropore structure of $ZTC_{(Co)}$-400-8h can provide more available channels for CO_2 diffusion and storage. Meanwhile, the $ZTC_{(Co)}$-400-8h contains more distortion locations and edge termination sites, which might change the electron density of the pore channel surface and enhance the electrostatic adsorption capacity. Investigating the strength of interaction between CO_2 molecules and $ZTC_{(Co)}$-400-B samples, the isosteric heat of adsorption (Q_{st}) was calculated by fitting CO_2 adsorption isotherms at 0, 25 and 50 °C for each sample (Fig. 6g). The stability of Q_{st} value at the initial adsorption stage (0.1-0.5 mol CO_2 small loading) reflects the excellent interaction strength between CO_2 and all sorbent samples. In contrast, the Q_{st} (ca. 26 kJ mol⁻¹) of $ZTC_{(Co)}$-400-8h is slightly
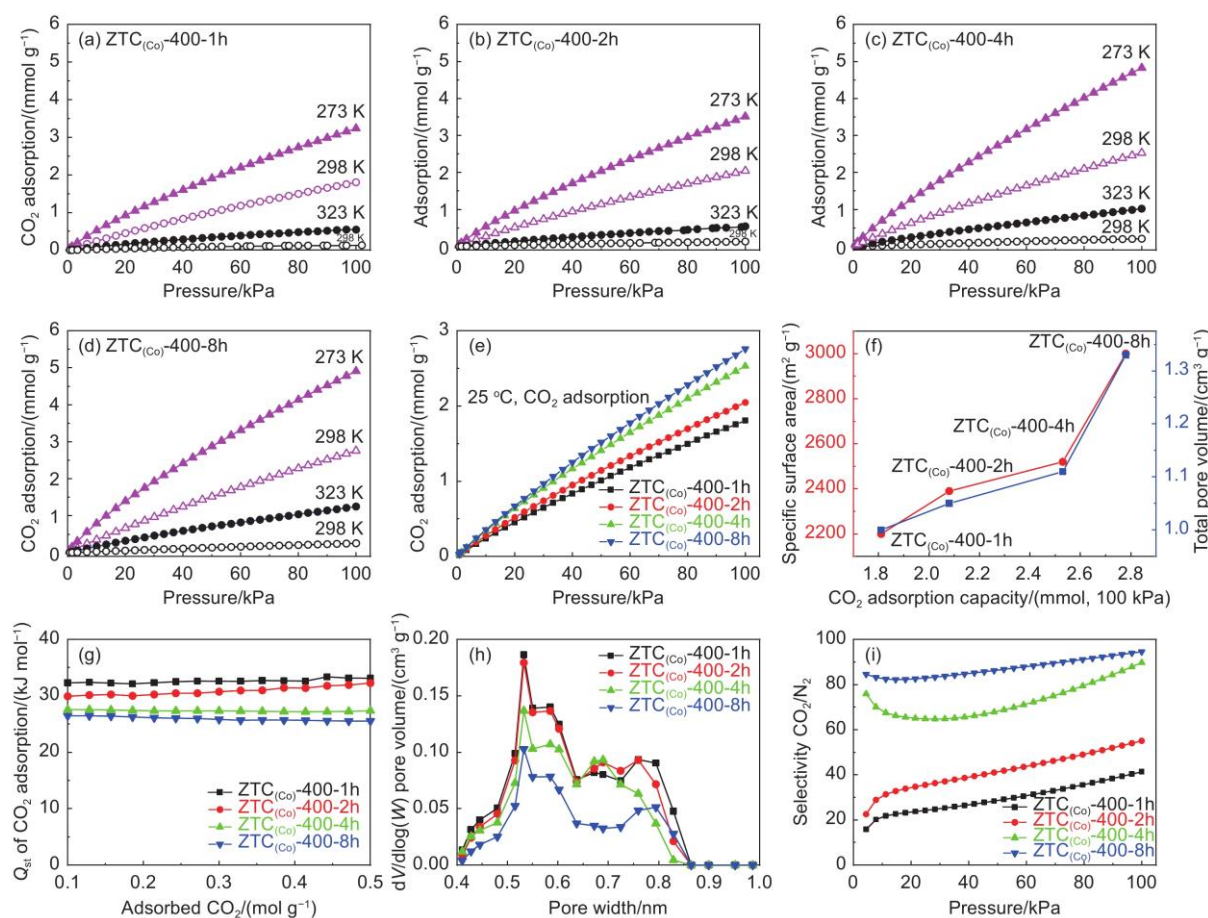

Fig. 6　(a-d) CO₂ adsorption isotherms (0, 25 and 50 °C) and N₂ adsorption isotherms (25 °C, black hollow circular). (e) Comparison of CO₂ adsorption properties at 25 °C. (f) Analysis of the plot of CO₂ adsorption capacity, specific surface area (red), and total pore volume (blue). (g) Isosteric heat of CO₂ adsorption (Q_{st}). (h) Pore size distribution (0.4-1.0 nm) derived from CO₂ adsorption isotherm (0 °C) by NLDFT method. (i) CO₂/N₂ selectivity calculated using IAST at 25 °C

lower than other samples. The reason may be that the $ZTC_{(Co)}$-400-8h has the more complete 3D ordered microporous channels and lacks the small micropore (0.4-0.9 nm) caused by the pore structural collapse. The PSDs derived from CO_2 adsorption isotherm (0 °C) are shown in Fig. 6h. The micropores (0.4-0.9 nm) in the $ZTC_{(Co)}$-400-8h are less than the other samples. However, the heat of gas adsorption has a significant positive correlation with the content of micropores within 0.4-0.8 nm[53]. Fig. 6i shows the selectivity of $ZTC_{(Co)}$-400-B samples for mixed gases of CO_2/N_2 with a volume ratio of 15/85 using IAST[37]. All $ZTC_{(Co)}$-400-B samples show a growing tendency of CO_2 selectivity with increasing pressure. $ZTC_{(Co)}$-400-8h contains the most significant SSA and the best-ordered microporous structure among the tested samples. Its CO_2 selectivity reached 98%, significantly higher than the other samples. Meanwhile, as an unmodified pure carbon material, $ZTC_{(Co)}$-400-8h has higher CO_2 capacity and selectivity than some pure/heteroatom-doped carbon material under atmospheric pressure due to its good structural characteristics[54-57], which makes it a potential adsorbent for CO_2 removal from N_2 in post-combustion flue gases.

3.6 ZTCs preparation on a large scale

Owing to the advantages of low synthesis temperature and simple CVD technology, it is promising to realize a large-scale synthesis of ZTCs by the present method. Herein, the amount of CoY zeolite template was increased from 0.4 to 10.0 g for batch production of ZTCs. The CVD using a mixture gas of Ar (30 mL min^{-1})/C_2H_2 (30 mL min^{-1}) with a high acetylene ratio was carried out for 8.0 h. Fig. 7a-e show photographs of the CoY zeolite bed before and after the CVD. After CVD, the black powders in the quartz boat indicate that an effective carbon deposition on large amounts of CoY templates could be achieved, although the amount of CoY zeolite was increased by 25 times. It can be noted from Fig. 7c-d that the quartz tube wall remains transparent even after 8.0 h acetylene CVD, suggesting that good catalytic activity of CoY zeolite could ensure a large number of carbons deposited into the template. According to the TGA results (Fig. S10), the carbon deposition of C/CoY-400-8h(L) is approximately 23.4% (mass fraction), which is enough to construct an ordered carbon framework, the production of $ZTC_{(Co)}$-400-8h(L) is ca. 3.0 g after the acid treatment. The XRD pattern (Fig. 7f) is much similar to that of the $ZTC_{(Co)}$-400-8h small-batch prepared, suggesting an ordered microporous structure of the sample. The SSA and pore volume (Fig. S11) of $ZTC_{(Co)}$-400-8h(L) is 2700 m^2 g^{-1} and 1.27 cm^3 g^{-1}, respectively. Table S3 summarizes the synthesis temperature, using the amount of template and parameters of ZTCs as prepared by the CVD method reported in the literature. The present technology to produce ZTCs has the advantages of the lowest CVD temperature, higher yield, and good quality. Therefore, it is highly promising to produce zeolite-templated carbon materials for mass production in a simple but energy-efficient way.
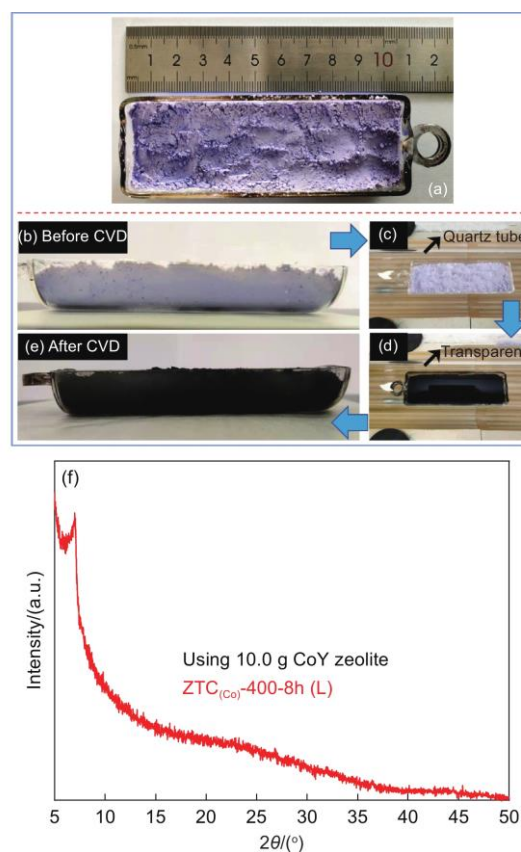

Fig. 7 (a-e) Photographs of quartz reactor for large-scale synthesis filled with a thick bed of CoY zeolite (10.0 g) sample. (f) XRD pattern of $ZTC_{(Co)}$-400-8h(L)

4 Conclusions

A large-scale technology to synthesize the ordered microporous carbon by acetylene CVD at a temperature as low as 400 °C using Co ion-exchanged zeolite as the template has been successfully developed. As the catalytic sites, the Co ions embedded into the template could make acetylene decompose and selectively deposited in zeolite pores at low temperatures to avoid the unselective deposition of carbons on the outer surface of the template by traditional high-temperature CVD. Furthermore, increasing the CVD time could improve the carbon content and stability of the ordered microporous carbon skeleton in the zeolite template optimal sample of $ZTC_{(Co)}$-400-8h owns a 3D-ordered microporous structure, large surface area (3 000 m^2 g^{-1}), and pore volume (1.33 cm^3 g^{-1}). Owing to the highly ordered pore structure, $ZTC_{(Co)}$-400-8h is a potential adsorbent for CO_2 capture, the uptake of CO_2 and CO_2/N_2 selectivity is 2.78 mmol g^{-1} (25 °C, 100 kPa) and 98%, respectively. In order to increase the potential for commercial application of this technology, the synthesis of high-quality ZTCs on a large scale by using a 10.0-g batch of CoY zeolite has been demonstrated successfully. In summary, the present technology to produce ZTCs has the advantages of low synthesis temperature, suitable for large-scale synthesis, and is easy to control.

Data availability statement

Acknowledgements

References

[1] Iijima S. Helical microtubules of graphitic carbon[J]. Nature, 1991, 354: 56-58.

[2] Geim A K. Graphene: status and prospects[J]. Science, 2009, 324: 1530-1534.

[3] Wang A M, Ren J W, Shi B F, et al. A facile one-pot synthesis of mesoporous graphite-like carbon through the organic-organic co-assembly[J]. Microporous and Mesoporous Materials, 2012, 151(15): 287-292.

[4] Liu W L, Du L Y, Ju S L, et al. Encapsulation of red phosphorus in carbon nanocages with ultrahigh content for high-capacity and long cycle life sodium-ion batteries[J]. ACS Nano, 2021, 15(3): 5679-5688.

[5] Liu L, Kan Y Y, Gao K, et al. Graphdiyne derivative as multifunctional solid additive in binary organic solar cells with 17. 3% efficiency and high reproductivity[J]. Advanced Materials, 2020, 32(11): 1907604.

[6] Zhao H W, Xing T Y, Li L X, et al. Synthesis of cobalt and nitrogen co-doped carbon nanotubes and its ORR activity as the catalyst used in hydrogen fuel cells[J]. International Journal of Hydrogen Energy, 2019, 44(44): 25180-25187.

[7] An B G, Xu S F, Li L X, et al. Carbon nanotubes coated with a nitrogen-doped carbon layer and its enhanced electrochemical capacitance[J]. Journal of Materials Chemistry A, 2013, 1(24): 7222-7228.

[8] Mauter M S, Elimelech M. Environmental applications of carbon-based nanomaterials[J]. Environmental Science & Technology, 2008, 42(16): 5843-5859.

[9] Graboski A M, Zakrzevski C A, Shimizu F M, et al. Electronic nose based on carbon nanocomposite sensors for clove essential oil detection[J]. ACS Sensors, 2020, 5(6): 1814-1821.

[10] Zhu C Y, Ye Y W, Guo X, et al. Design and synthesis of carbon-based nanomaterials for electrochemical energy storage. New Carbon Materials, 2022, 37(1): 59-92.

[11] Zhou Y, Jia Z X, Zhao S Y, et al. Construction of triple-shelled hollow nanostructure by confining amorphous Ni-Co-S/crystalline MnS on/in hollow carbon nanospheres for all-solid-state hybrid supercapacitors[J]. Chemical Engineering Journal, 2021, 416(15): 129500.

[12] Li X Y, Sari H M K, Niu L J, et al. Porous graphene nanocages with wrinkled surface enhancing electrocatalytic activity of lithiun/sulfuryl chloride batteries[J]. RSC Advances, 2021, 11(16): 9469-9475.

[13] Zhang X L, Ruan Z Q, He Q T, et al. Three-dimensional (3D) nanostructure skeleton substrate composed of hollow carbon fiber/carbon nanosheet/ZnO for stable lithium anode[J]. ACS Applied Materials & Interfaces, 2021, 13(2): 3078-3088.

[14] Cheng H Y, Cheng P Y, Chuah X F, et al. Porous N-doped carbon nanostructure integrated with mesh current collector for Li-ion based energy storage[J]. Chemical Engineering Journal, 2019, 374(15): 201-210.

[15] Zhao H W, Zhang Y Q, Li L X, et al. Synthesis of an ordered porous carbon with the dual nitrogen-doped interface and its ORR catalysis performance[J]. Chinese Chemical Letters, 2021, 32(1): 140-145.

[16] Zhu Y, Miyake K, Shu Y, et al. Single atomic Co coordinated with N in microporous carbon for oxygen reduction reaction obtained from Co/2-methylimidazole anchored to Y zeolite as a template[J]. Materials Today Chemistry, 2021, 20: 100410.

[17] Konnov S V, Dubray F, Clatworthy E B, et al. Novel strategy for the synthesis of ultra-stable single-site Mo-ZSM-5 zeolite nanocrystals[J]. Angewandte Chemie International Edition, 2020, 59(44): 19553-19560.

[18] Cui X X, Xu Y S, Chen L L, et al. Ultrafine Pd nanoparticles supported on zeolite-templated mesocellular graphene network via framework aluminum mediation: an advanced oxygen reduction electrocatalyst[J]. Applied Catalysis B: Environmental, 2019, 244: 957-964.

[19] Nueangnoraj K, Ruiz-Rosas R, Nishihara H, et al. Carbon–carbon asymmetric aqueous capacitor by pseudocapacitive positive and stable negative electrodes[J]. Carbon, 2014, 67: 792-794.

[20] Nomura K, Nishihara H, Yamamoto M, et al. Force-driven reversible liquid–gas phase transition mediated by elastic nanosponges[J]. Nature Communications, 2019, 10: 2559.

[21] Tang R, Taguchi K, Nishihara H, et al. Insight into the origin of carbon corrosion in positive electrodes of supercapacitors. Journal of Materials Chemistry A, 2019, 7(13): 7480-7488.

[22] Dubey R J C, Nüssli J, Piveteau L, et al. Zeolite-templated carbon as the cathode for a high energy density dual-ion battery[J]. ACS Applied Materials & Interfaces, 2019, 11(19): 17686-17696.

[23] Itoi H, Nishihara H, Kogure T, et al. Three-dimensionally arrayed and mutually connected 1. 2-nm nanopores for high-performance electric double layer capacitor[J]. Journal of the American Chemical Society, 2011, 133(5): 1165-1167.

[24] Choi S, Kim H, Lee S, et al. Large-scale synthesis of high-quality zeolite-templated carbons without depositing external carbon layers[J]. Chemical Engineering Journal, 2015, 280(15): 597-605.

[25] Nishihara H, Kyotani T. Zeolite-templated carbons-three-dimensional microporous graphene frameworks[J]. Chemical

Communications, 2018, 54(45): 5648-5673.

[26] Kyotani T, Nagai T, Inoue S, et al. Formation of new type of porous carbon by carbonization in zeolite nanochannels[J]. Chemistry of Materials, 1997, 9(2): 609-615.

[27] Matsuoka K, Yamagishi Y, Yamazaki T, et al. Extremely high microporosity and sharp pore size distribution of a large surface area carbon prepared in the nanochannels of zeolite Y[J]. Carbon, 2005, 43(3): 876-879.

[28] Ma Z X, Kyotani T, Tomita Akira. Preparation of a high surface area microporous carbon having the structural regularity of Y zeolite[J]. Chemical Communication, 2000, 2365-2366.

[29] Ma Z X, Kyotani T, Tomita Akira. Synthesis methods for preparing microporous carbons with a structural regularity of zeolite Y[J]. Carbon, 2002, 40(13): 2367-2374.

[30] Hou P X, Yamazaki T, Orikasa H, et al. An easy method for the synthesis of ordered microporous carbons by the template technique[J]. Carbon, 2005, 43(12): 2624-2627.

[31] Zhao H W, Li L X, Liu Y Y, et al. Synthesis and ORR performance of nitrogen-doped ordered microporous carbon by CVD of acetonitrile vapor using silanized zeolite as template[J]. Applied Surface Scienve, 2020, 504(28): 144438.

[32] Kim K, Lee T, Kwon Y, et al. Lanthanum-catalysed synthesis of microporous 3D graphene-like carbons in a zeolite template[J]. Nature, 2016, 535: 131-135.

[33] Kim K, Kwon Y, Lee Y, et al. Facile large-scale synthesis of three-dimensional graphene-like ordered microporous carbon via ethylene carbonization in CaX zeolite template[J]. Carbon 2017, 118: 517-523.

[34] Moon G H, Bähr A, Tüysüz H. Structural engineering of 3D carbon materials from transition metal ion-exchanged Y zeolite templates[J]. Chemistry of Materials, 2018, 30(11): 3779-3788.

[35] Han J, Zhang L, Zhao B, et al. The N-doped activated carbonderived from sugarcane bagasse for CO_2 adsorption[J]. Industrial Crops and Products, 2019, 128: 290-297.

[36] Bhadra B N, Seo P W, Jhung S H. Adsorption of diclofenac sodium from water using oxidized activated carbon[J]. Chemical Engineering Journal, 2016, 301(1): 27-34.

[37] Jin Q Q, Fang D, Ye Y L, et al. Cu, Co, or Ni species in exchanged Y zeolite catalysts and their denitration performance for selective catalytic reduction by ammonia[J]. Applied Surface Science, 2022, 600(30): 154075.

[38] Shilina M I, Rostovshchikova T N, Nikolaev S A, et al. Polynuclear Co-oxo cations in the catalytic oxidation of CO on Co-modified ZSM-5 zeolites[J]. Materials Chemistry and Physics, 2019, 223(1): 287-298.

[39] Balahmar N, Lowbridge A M, Mokaya R. Templating of carbon in zeolites under pressure: synthesis of pelletized zeolite templated carbons with improved porosity and packing density for superior gas (CO_2 and H_2) uptake properties[J]. Journal of Materials Chemistry A, 2016, 4(37): 14254-14266.

[40] Nishihara H, Ittisanronnachai S, Itoi H, et al. Experimental and theoretical studies of hydrogen/deuterium spillover on Pt-loaded zeolite-templated carbon[J]. The Journal of Physical Chemistry C, 2014, 118(18): 9551-9559.

[41] Konwar R J, De M. Effects of synthesis parameters on zeolite templated carbon for hydrogen storage application[J]. Microporous and Mesoporous Materials, 2013, 175(15): 16-24.

[42] Ania C O, Khomenko V, Raymundo-Piñero E, et al. The large electrochemical capacitance of microporous doped carbon obtained by using a zeolite template[J]. Advanced Functional Materials, 2007, 17(11): 1828-1836.

[43] Yang Z X, Xia Y D, Mokaya R. Hollow shells of high surface area graphitic N-doped carbon composites nanocast using zeolite templates[J]. Microporous and Mesoporous Materials, 2005, 86(1-3): 69-80.

[44] Eveleens C A, Irle S, Page A J. How does acetonitrile modulate single-walled carbon nanotube diameter during CVD growth[J]. Carbon, 2019, 146: 535-541.

[45] Miao Z C, Meng J, Liang M F, et al. In-situ CVD synthesis of Ni@N-CNTs/carbon paper electrode for electro-reduction of CO_2[J]. Carbon, 2021, 172: 324-333.

[46] Itoi H, Kasai Y, Morishita K, et al. Facile synthesis of high surface area zeolite-templated carbons using divinyblenzene and propylene as carbon sources[J]. Microporous and Mesoporous Materials, 2021, 326: 111378.

[47] Zaretskiy S N, Hong Y K, Ha D H, et al. Growth of carbon nanotubes from Co nanoparticles and C_2H_2 by thermal chemical vapor deposition[J]. Chemical Physics Letters, 2003, 372(1-2): 300-305.

[48] Nishihara H, Fujimoto H, Itoi H, et al. Graphene-based ordered framework with a diverse range of carbon polygons formed in zeolite nanochannels[J]. Carbon, 2018, 129: 854-862.

[49] Madison L, Heitzer H, Russell C, et al. Atomistic simulations of CO_2 and N_2 within cage-type silica zeolites[J]. Langmuir, 2011, 27(5): 1954-1963.

[50] Mehio N, Dai S, Jiang D. Quantum mechanical basis for kinetic diameters of small gaseous molecules[J]. The Journal of Physical Chemistry A, 2014, 118(6): 1150-1154.

[51] Sakamoto H, Fujimori T, Li X L, et al. Cycloparaphenylene as a molecular porous carbon solid with uniform pores exhibiting adsorption-induced softness[J]. Chemical Science, 2016, 7(7): 4204-4210.

[52] Zhang Y Y, Zhang S N, Wang Z C, et al. Determination of the absolute CH_4 adsorption using simplified local density theory and compariosn with the modified Langmuir adsorption model[J]. RSC Advances, 2018, 8(72): 41509-41516.

[53] Li H J, Wang S C, Zeng Q, et al. Effects of pore structure of different rank coals on methane adsorption heat[J]. Processes, 2021, 9(11): 1971.

[54] García-Díez E, Castro-Muñiz A, Paredes J I, et al. CO_2 capture by novel hierarchical activated ordered micro-mesoporous carbons derived from low value coal tar products[J]. Microporous and Mesoporous Materials, 2021, 318: 110986.

[55] Wang X J, Yuan B Q, Zhou X, et al. Novel glucose-based adsorbents (Glc-Cs) with high CO_2 capacity and excellent $CO_2/CH_4/N_2$ adsorption selectivity[J]. Chemical Engineering Journal, 2017, 327: 51-59.

[56] Li D, Chen Y L, Zheng M, et al. Hierarchically structured porous

nitrogen-doped carbon for highly selective CO_2 capture[J]. ACS Sustainable Chemistry & Engineering, 2016, 4(1): 298-304.

[57] Kim Y K, Kim G M, Lee J W. Highly porous N-doped carbons impregnated with sodium for efficient CO_2 capture[J]. Journal of Materials Chemistry A, 2015, 3(20): 10919-10927.